Clusters in an Epidemic Model with Long-Range Dispersal

Xiangyu Cao,[1] Pierre Le Doussal,[1] and Alberto Rosso[2]
[1]Laboratoire de Physique de l'École normale supérieure, ENS, Université PSL, CNRS, Sorbonne Université, Université Paris Cité, F-75005 Paris, France
[2]Université Paris-Saclay, CNRS, LPTMS, 91405 Orsay, France

(Received 5 April 2022; revised 27 May 2022; accepted 17 August 2022; published 1 September 2022)

In the presence of long-range dispersal, epidemics spread in spatially disconnected regions known as clusters. Here, we characterize exactly their statistical properties in a solvable model, in both the supercritical (outbreak) and critical regimes. We identify two diverging length scales, corresponding to the bulk and the outskirt of the epidemic. We reveal a nontrivial critical exponent that governs the cluster number and the distribution of their sizes and of the distances between them. We also discuss applications to depinning avalanches with long-range elasticity.

DOI: 10.1103/PhysRevLett.129.108301

Catastrophic events such as avalanches, material failure, and initial-stage epidemic outbreaks often occur as a chain reaction. Their simplest model was that of Bienaymé and Galton-Watson (BGW) [1,2], originally conceived for genealogy. In a continuous time version one starts with a single infected individual. During a short time lapse $\mathrm{d}t$ each infected individual recovers with probability $\gamma \mathrm{d}t$, and causes a new infection with probability $\beta \mathrm{d}t$. On average, each infection generates $R_0 = \beta/\gamma$ new ones: R_0 determines the fate of the epidemic. When $R_0 < 1$, it goes to extinction rapidly. When $R_0 > 1$, the size of the population that has been infected up to time t grows exponentially, $S \sim e^{(\beta-\gamma)t}$, as in the initial outbreak stage of an epidemic. At the critical point, $R_0 = 1$, the probability that the epidemic has survived up to time t decreases as $\sim 1/t$, and in that case it will have infected $\sim t^2$ individuals. As a result, S has strong fluctuations and has a power law distribution $P(S) \sim S^{-3/2}$ with a cutoff at $S_{\max} \sim t^2$. The critical case mimics the scale free behavior displayed by avalanches in disordered materials, i.e., the propagation of an instability which triggers further instabilities via elastic interaction [3].

The BGW model ignores the spatial spreading of the epidemic. Branching diffusion models consider that infected individuals also perform some random walk in a d dimensional space, independently of recovery and infection. Often, one specifies the random walk to be a short-range Brownian motion. Then the region affected by the epidemic is a connected set, whose geometric properties have been characterized [4–10]. For instance, at criticality, the radius ξ of this set grows as $\xi \sim S^{1/4}$.

However, Brownian diffusion models cannot capture the *long-range* dispersal that ubiquitously occurs in nature, due to, e.g., wind, ocean currents, and air traffic [11–17], spreading an epidemic far from its origin. A similar situation is observed in disordered materials where long-range interactions can trigger disconnected avalanches, e.g., in the propagation of crack fronts [18–21], wetting lines [22–24], or plasticity [25,26]. In this Letter, we model the long-range dispersal of the infected individuals as follows: during $\mathrm{d}t$, an individual jumps from x to x' with probability $p_\alpha(x - x')\mathrm{d}^d x' \mathrm{d}t$, where $p_\alpha(x)$ decays as a power law at large distances:

$$p_\alpha(x) = \frac{\theta(|x| - \epsilon)}{|x|^{\alpha+d}}, \qquad \alpha > 0. \tag{1}$$

Here $|x|$ is the Euclidean norm, θ is the Heaviside step function, and $\epsilon \ll 1$ is a short-distance cutoff. Similar long-range models have been studied on a lattice, where the outbreak always displays a subexponential growth [27–33]. Here, we assume an infinite pool of susceptible individuals everywhere, which ensures an exponential outbreak when $R_0 > 1$.

A typical epidemic obtained from a numerical simulation of our model is shown in Fig. 1. One may distinguish two regions characterized by distinct length scales. The *bulk*, of radius ξ, contains most of the infections. Farther away, a sparser *outskirt* of radius D contains all the remaining infections. The existence of the outskirt is a consequence of the long-range jumps. One aim of this Letter is to obtain how ξ and D scale with the infected population S. Another fundamental consequence of long-range dispersal is the presence of *clusters*, i.e., spatially disconnected regions affected by the epidemic. As is apparent from Fig. 1, the clusters vary in sizes, and their spatial distribution is not uniform. The second goal of this Letter is to introduce a method to properly define the clusters. We then characterize their random geometry: how the number of clusters grows with S, how their sizes are distributed, what distances are separating them, etc. Our exact results are obtained by the analysis of a nonlinear "instanton"

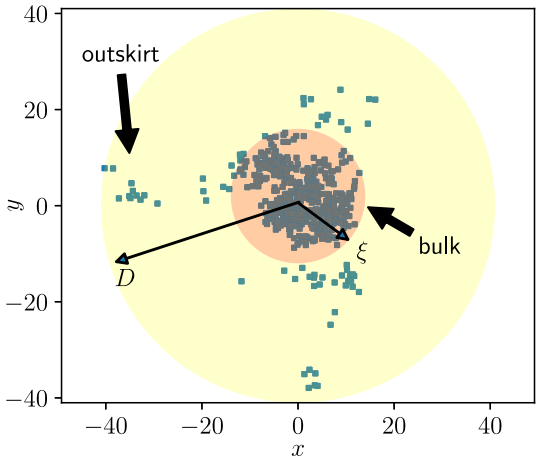

FIG. 1. Spatial distribution of a critical epidemic started at the origin, totaling 1000 infections. Because of the long-range dispersal [(1), $\alpha = 1.5$] of infected individuals, the points visited form disconnected clusters. The bulk of radius ξ, concentrating a majority of infections, is surrounded by a sparse outskirt, containing *all* infections.

equation. We stress that our methods are applicable to real-world data. As a proof of principle, we tested our theory against the Covid-19 outbreak data in the U.S. Remarkably, a prediction of our model, Eq. (12) below, describes well the spatial distribution of the clusters during the first week of March 2020 (see the Supplemental Material [34]).

The epidemic model introduced above provides a discrete realization, equivalent, near criticality [40], to the mean-field theory [41,42] describing the spatial structure of the avalanches of slowly driven elastic interfaces in a disordered medium. In crack experiments, clusters have been directly observed [43], and their number and size distribution have been characterized [44,45]. These works proposed that these properties are fully encoded in the global properties of the crack front, e.g., in its roughness exponent [46–48]. Here, we make a first step at examining this issue analytically; our results indicate that the cluster statistics probably involve a new independent exponent. In what follows, we report our main results, and sketch the main points of their derivation; see the Supplemental Material [34] for details.

Bulk and outskirt.—We first determine the length scales of the bulk ξ and outskirt D, by simple arguments. We consider our model with a single infected individual at the origin initially ($t = 0$). At criticality ($R_0 = 1$), the bulk length ξ can be estimated as the *typical* displacement of a random walk with jump distribution [Eq. (1)]. When $\alpha < 2$, we have a Lévy flight, and thus

$$\xi \sim t^{\frac{1}{\alpha}} \sim S^{\frac{1}{2\alpha}}, \qquad \alpha < 2, \tag{2}$$

where the last estimate comes from the scaling $S \sim t^2$. When $\alpha > 2$, we recover the short-range behavior $\xi \sim \sqrt{t} \sim S^{\frac{1}{4}}$ [42,49]. On the other hand, the outskirt's diameter D is estimated as the *farthest* jump among $\sim S$ independent attempts:

$$D \sim S^{\frac{1}{\alpha}}. \tag{3}$$

Hence, the outskirt is much larger than the bulk if $\alpha < 4$: only for $\alpha > 4$ do we completely recover a short-range behavior, with $D \sim \xi \sim S^{1/4}$. This is already a surprise, as naively one would expect a short-range takeover at $\alpha = 2$.

In the supercritical regime, the argument for the outskirt diameter D and the result [Eq. (3)] still hold. The scaling of the bulk size ξ is different. Indeed, the infected population grows exponentially, $S \sim e^{(\beta-\gamma)t}$. As a consequence, the density of infected individuals is exponentially large at the epicenter, $x = 0$, and decays as $\sim S|x|^{-\alpha-d}$ [Eq. (1)]. The bulk extent is then determined by the distance, $|x| = \xi$, at which the density reaches unity:

$$\xi \sim S^{\frac{1}{\alpha+d}} \sim e^{\frac{\beta-\gamma}{\alpha+d}t} \tag{4}$$

Note that, when $R_0 > 1$, the separation of scales $D \gg \xi$ remains for any α, and the short-range behavior with a linear growth $\xi \propto t$ is never recovered. This is in contrast with lattice models [27,28], where a reduction to short range does happen at $\alpha = d + 1$.

Defining clusters.—In our model, the ensemble of positions ever occupied by an infected individual up to time t is a finite set, as only a finite number of jumps have occurred. How do we define its clusters? For simplicity we focus on one and two dimensions. We introduce a coarse-graining scale $b \gg \epsilon$, and thicken each point by a patch of size b—an interval of length b in 1D, and a square of size b in 2D—centered at that point; see Fig. 2. The patches attached to different points can then overlap and form clusters. To characterize their spatial distribution, we introduce the following observables: (i) the number of clusters N_c; (ii) the length and area of individual clusters, ℓ_c in 1D and $\mathcal{A}_c$ in 2D, whereby the sum of all ℓ_c ($\mathcal{A}_c$) is the epidemic's *extension* ℓ (area, $\mathcal{A}$, respectively); and (iii) the distances between clusters. In 1D, a natural choice is the distribution of gaps (Fig. 2). It is not hard to see that the number of gaps larger than g is related to the cluster number with $b = g$:

$$N_c(b = g) = (\text{number of gaps} > g) + 1. \tag{5}$$

In 2D, the notion of gaps is not obvious, and we take $N_c(b = g)$ as a probe of the distances between clusters. We obtained the b dependence of all the quantities; for conciseness, we report results with $b = 1$ unless otherwise stated.

Clusters at criticality.—When $R_0 = 1$, statistical fluctuations are strong, and there are various ways of averaging. Here, we focus on averages conditioned on a large infected

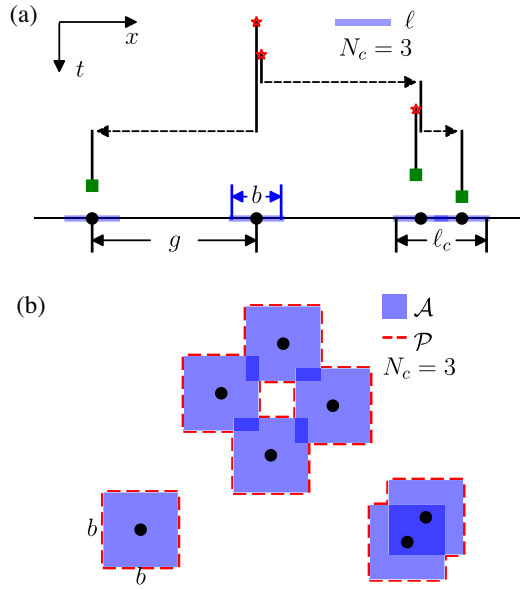

FIG. 2. (a) Illustration of an epidemic in 1D. An infection (recovery, jump) is indicated by a red star (green square, dashed line, respectively). The points visited are coarse grained by an interval of length b. They form $N_c = 3$ clusters, with total extension $\ell = \sum \ell_c$. The gaps g are defined independently of b. (b) In 2D, a point is coarse grained by a square of side b, to define the cluster number $N_c(= 3)$, the area $\mathcal{A}$, and the perimeter $\mathcal{P}$. Note that in 2D, a cluster can be nonconvex and have holes.

population S (assuming nonextinction), denoted as $\langle \mathcal{O} \rangle_S$ for an observable $\mathcal{O}$. From the S-conditioned averages, we can obtain the asymptotics of the average over all realizations up to time t, using

$$\langle \mathcal{O}(t) \rangle \sim \int^{S_{\max}} P(S) \langle \mathcal{O} \rangle_S \mathrm{d}S, \qquad S_{\max} \sim t^2. \tag{6}$$

Thus, if $\langle \mathcal{O} \rangle_S \sim S^a$, $\langle \mathcal{O}(t) \rangle \sim t^{\max(2a-1,0)}$ (See Table I of the Supplemental Material [34] for results).

We have seen that when $\alpha < 4$, the outskirt is much larger than the bulk, and we expect many clusters. Interestingly, the interval $\alpha \in (0, 4)$ is divided into several regimes, with qualitatively different behaviors of $\langle \ell \rangle_S$, $\langle \mathcal{A} \rangle_S$, and $\langle N_c \rangle_S$. Let us start with the most nontrivial one, $\alpha \in (d/2, d)$. There, we find that the average extension and area are related to the bulk extent in a rather expected way:

$$\langle \ell \rangle_S \sim \xi, \qquad \langle \mathcal{A} \rangle_S \sim \xi^2. \tag{7}$$

It is worth noting that the above quantities are independent of b for a large range of b; see Eq. (15) below. Now, the average number of clusters scales with ξ via a new and nontrivial exponent

$$\langle N_c \rangle_S \sim \xi^{\chi}, \qquad \alpha < \chi < d. \tag{8}$$

The exponent χ is a function of α and d, and determined by a transcendental equation given in the Supplemental Material [34] together with a plot. It satisfies $\alpha < \chi < d$, which means that the number of clusters grows with S but remains much lower than the area or extension. Thus, the cluster areas $\mathcal{A}_c$ and extensions ℓ_c must have broad distributions (with divergent mean as $S \to \infty$). Computing them is beyond the reach of the present techniques. However, assuming that they follow a single power law in the interval $[1, \xi^d]$, we can surmise their exponent [45]:

$$P(\ell_c) \sim \ell_c^{-\chi-1}, \qquad P(\mathcal{A}_c) \sim \mathcal{A}_c^{-\chi/2-1}. \tag{9}$$

Concerning the gaps between clusters, we found that $\langle N_c(b = g) \rangle_S$ has two regimes with distinct power laws:

$$\frac{\langle N_c(b=g) \rangle_S}{\sqrt{S}} \sim \begin{cases} (g/g_c)^{-\frac{d(\chi-\alpha)}{d-\alpha}} & 1 \ll g \ll g_c \\ (g/g_c)^{-\frac{\alpha d}{d+\alpha}} & g_c \ll g \ll D \end{cases}, \tag{10}$$

where $g_c = \xi^{1-\alpha/d}$ is the crossover gap length. The two gap regimes $g \ll g_c$ and $g \gg g_c$ correspond to gaps in the bulk and in the outskirt, respectively. To better understand this result, let us consider one dimension [50]. Observe that the total length of the gaps no greater than g_c is exactly the bulk size:

$$\sum (\text{gaps} \le g_c) \sim g_c \langle N_c(b = g_c) \rangle_S \sim \xi. \tag{11}$$

Now, if we consider all the bulk gaps up to a size $g \ll g_c$, their number is almost $N_c(b = 1)$, but their total size is a negligible fraction of the bulk. On the other hand, the outskirt gaps are a minority in number, but their total size is much greater than the bulk size. Of course, there is no sharp transition between bulk and outskirt, but rather a smooth crossover. Indeed, in Fig. 3, we show that to demarcate the two power laws requires several orders of g/g_c. Otherwise, one may observe a "compromise" of the theoretical predictions.

So far we focused on the regime $\alpha \in (d/2, d)$. The other ones are simpler. In a nutshell, for strong long-range dispersal ($\alpha < d/2$), the clusters become atomic and have a finite size on average. Therefore we have $\langle N_c \rangle_S \sim S$, and $\langle \ell \rangle_S, \langle \mathcal{A} \rangle_S \sim S$ as well. For weak long-range dispersal ($\alpha > d$), the bulk becomes more compact, and gaps of size $\gtrsim 1$ exist only in the outskirt. See the Supplemental Material [34] for a detailed discussion.

Clusters of an outbreak.—In the supercritical ($R_0 > 1$) regime, the statistical fluctuations are weak. We can thus consider the averages up to t, which are dominated by realizations with an infected population $S \sim e^{(\beta-\gamma)t}$. Recall that the bulk and outskirt diameter grow exponentially as Eqs. (3) and (4), for any $\alpha > 0$. Now, the cluster structure of an outbreak is also simpler, and we found the same qualitative picture for any α. The bulk is compact and has no large gaps. Its extension is $\langle \ell \rangle \sim \xi$, $\langle \mathcal{A} \rangle \sim \xi^2$, where $\xi \sim S^{1/(d+\alpha)} \sim e^{(\beta-\gamma)t/(d+\alpha)}$ [Eq. (4)]. The outskirt is sparse, and has an exponential number of clusters, $\langle N_c \rangle \sim \xi^d$.

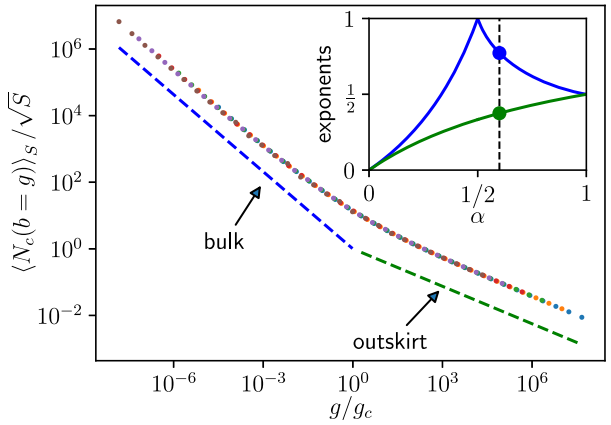

FIG. 3. Gap distribution in 1D with $\alpha = 0.6$, obtained by numerical solution of Eq. (13) [34]. Data points with various sizes $S = 10^{20}, \ldots, 10^{28}$ are collapsed using Eq. (10). The dashed lines indicate the predicted exponents in two regimes. Inset: dependence of the two exponents on α.

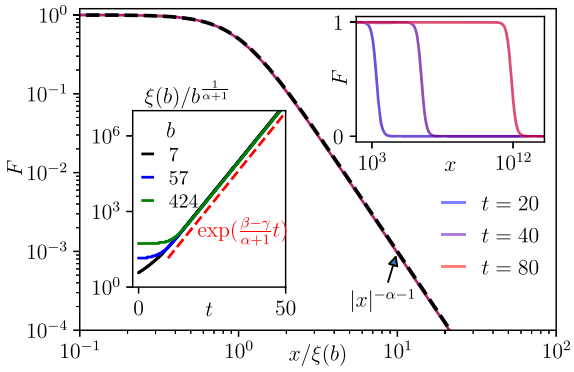

FIG. 4. Traveling wave solution to Eq. (13) in the supercritical regime ($\alpha = 2, \beta = 1, \gamma = 0, b = 7$). The solution at $t = 20$, 40, 80 (upper inset) collapsed onto the front profile $F(x,t) = f[x/\xi(b)]$, $f(y) = 1/(1+y^{1+\alpha})$ (black dashed curve). The front position $\xi(b)$ is defined by $F[\xi(b)] = 1/2$. Its time dependence is plotted in the lower inset for three values of b. The collapse confirms the b dependence of the front position [34].

Notably, their spatial structure is time independent: the gap distribution is stationary up to a normalization and a cutoff,

$$\langle N_c(b=g)\rangle \sim \xi^d g^{-\frac{d\alpha}{\alpha+d}}, \qquad g \ll D. \tag{12}$$

In the Supplemental Material [34], we tested this prediction against Covid-19 data, finding an encouraging agreement.

Method.—We highlight some key points of our analytical approach. The main object is a function $F(x,t|b)$, which is the probability that x belongs to the patch of some point visited before t. A standard backward recursion argument shows that F satisfies a semilinear "instanton" equation [42,51–54]:

$$\partial_t F = \mathcal{D}^\alpha F + (\beta-\gamma)F - \beta F^2, \qquad F|_{t=0} = 0, \tag{13}$$

for any x outside the patch of the origin; inside that, $F = 1$. Here $(\mathcal{D}^\alpha f)(x) \coloneqq \int p_\alpha(x-y)[f(y)-f(x)]\mathrm{d}^d y$ is the "fractional diffusion" term. From the solution F, we can obtain the area (extension) by integrating it over the plane (line). The cluster number is obtained by differentiating with respect to b. In 1D, we have

$$N_c(b) = \partial_b \ell(b). \tag{14}$$

A similar trick exists in 2D [34].

Therefore, the problem boils down to the asymptotic analysis of Eq. (13). In the supercritical regime, the exponential spreading of its traveling wave solution follows from existing rigorous results [55]; for a self-contained derivation and our results on clusters, see the Supplemental Material [34]. In Fig. 4, we plot the front profile. Note that it decays as a power law, and does not have a characteristic width. In contrast, in traveling wave equations with short-range diffusion, the wavefront position has linear growth in time, and its width is of order unity.

The results at criticality follow from the stationary solution of Eq. (13). The solution in the regime $\alpha \in (d/2, d)$ involves a noteworthy feature. To discuss that without going into technical details, consider the following puzzle, say in 1D. Recall that the cluster number and the extension are related by a b derivative Eq. (14). Then, how can they scale differently: $\ell \sim \xi$, $N_c \sim \xi^\chi \ll \xi$? The crux is that the leading asymptotics of ℓ is b independent, while N_c derives from a subleading term:

$$\langle \ell(b)\rangle_S = c_0\xi + c_1(b)\xi^\chi, \qquad (b \ll g_c) \tag{15}$$

where c_0 is b independent. To extract the cluster statistics from the solution of Eq. (13), it is necessary to identify its *subleading* asymptotics, in addition to the previously known leading one [56]. This mathematical detail has a physical interpretation: cluster statistics are associated with irrelevant perturbations in the sense of the renormalization group. During the coarse-graining process, the clusters merge, and information about them is gradually erased.

Conclusion.—We have characterized the clusters of an epidemic model with long-range dispersal, which is equivalent near criticality to the mean-field theory of depinning avalanches with long-range elasticity. We found that two diverging length scales—the bulk and the outskirt—emerge in both supercritical and critical regimes. In the latter, the bulk can have a rich structure with broadly distributed cluster sizes as well as gap sizes. Our analytical approach based on the instanton equation can be extended to study the effect of inhomogeneous networks [14], realistic mixing patterns [14,57], superspreading events [58], or the regions where the epidemic is still active at time t [59,60]. It will be also interesting to see how much the qualitative features revealed here appear in other epidemic models, e.g., contact point processes [61,62]. Finally, concerning depinning

avalanches, our model provides a mean-field description which should be quantitatively correct for realistic long-range systems when $d \geq 2\alpha$. To describe these systems for $d < 2\alpha$, loop corrections to mean-field theory should be taken into account. In particular, our results imply a cluster number distribution $P(N_c) \sim N_c^{-\mu}$ where $\mu = \alpha/\chi + 1$ for $\alpha \in (d/2, d)$. At the critical dimension $d = 2\alpha$, we recover the BGW value $\mu = 3/2$, but in our model $\mu > 3/2$ is a new exponent when $d < 2\alpha$. Meanwhile, numerical studies [45] of realistic models suggest that $\mu \approx 3/2$ for all $d < 2\alpha$. It will be interesting to see how to retain the "dangerously irrelevant" cluster statistics in the field theory and whether the loop corrections can account for this numerical observation.

We thank Jean-Philippe Bouchaud for pointing out the literature on human mobility. We thank William Terrot for preliminary work on the project, and Grégory Schehr, Vincenzo Schimmenti for valuable comments on the manuscript. P. L. D. acknowledges support from ANR under Grant No. ANR-17-CE30-0027-01 RaMaTraF [63].

[1] I. J. Bienaymé, De la loi de multiplication et de la durée des familles, Soc. Philomat. Paris Extraits, Sér **5**, 37 (1845); L'institut**589**, 13:131 (1975); Reprinted in D. G. Kendall, The genealogy of genealogy: Branching processes before (and after) 1873, Bull. London. Math. Soc. **7**, 225 (1975).
[2] H. Watson and F. Galton, On the probability of the extinction of families, J. Anthropol. Inst. G. B. Irel. **4**, 138 (1875), https://www.jstor.org/stable/pdf/2841222.pdf.
[3] Bruno Alessandro, Cinzia Beatrice, Giorgio Bertotti, and Arianna Montorsi, Domain-wall dynamics and barkhausen effect in metallic ferromagnetic materials. I. Theory, J. Appl. Phys. **68**, 2901 (1990).
[4] Maury D. Bramson, Maximal displacement of branching brownian motion, Commun. Pure Appl. Math. **31**, 531 (1978).
[5] Gordon Slade, Scaling limits and super-brownian motion, Not. Am. Math. Soc. **49**, 1056 (2002), https://www.ams.org/notices/200209/fea-sladecolor.pdf.
[6] É. Brunet and B. Derrida, Statistics at the tip of a branching random walk and the delay of traveling waves, Europhys. Lett. **87**, 60010 (2009).
[7] Louis-Pierre Arguin, Anton Bovier, and Nicola Kistler, The extremal process of branching brownian motion, Probab. Theory Relat. Fields **157**, 535 (2013).
[8] Eric Dumonteil, Satya N. Majumdar, Alberto Rosso, and Andrea Zoia, Spatial extent of an outbreak in animal epidemics, Proc. Natl. Acad. Sci. U.S.A. **110**, 4239 (2013).
[9] Kabir Ramola, Satya N. Majumdar, and Grégory Schehr, Spatial extent of branching brownian motion, Phys. Rev. E **91**, 042131 (2015).
[10] Kabir Ramola, Satya N. Majumdar, and Grégory Schehr, Universal Order and Gap Statistics of Critical Branching Brownian Motion, Phys. Rev. Lett. **112**, 210602 (2014).
[11] Andrew V. Suarez, David A. Holway, and Ted J. Case, Patterns of spread in biological invasions dominated by long-distance jump dispersal: Insights from argentine ants, Proc. Natl. Acad. Sci. U.S.A. **98**, 1095 (2001).
[12] James K. M. Brown and Mogens S. Hovmøller, Aerial dispersal of pathogens on the global and continental scales and its impact on plant disease, Science **297**, 537 (2002).
[13] Ran Nathan, Long-distance dispersal of plants, Science **313**, 786 (2006).
[14] Dirk Brockmann, Human mobility and spatial disease dynamics, in *Reviews of Nonlinear Dynamics and Complexity* (John Wiley & Sons, Ltd, New York, 2009), Chap. 1, pp. 1–24.
[15] Marta C. González, César A. Hidalgo, and Albert-László Barabási, Understanding individual human mobility patterns, Nature (London) **453**, 779 (2008).
[16] Prasad Perlekar, Roberto Benzi, David R. Nelson, and Federico Toschi, Population Dynamics at High Reynolds Number, Phys. Rev. Lett. **105**, 144501 (2010).
[17] Vittoria Colizza, Alain Barrat, Marc Barthélemy, and Alessandro Vespignani, The role of the airline transportation network in the prediction and predictability of global epidemics, Proc. Natl. Acad. Sci. U.S.A. **103**, 2015 (2006).
[18] J. R. Rice, First-order variation in elastic fields due to variation in location of a planar crack front, J. Appl. Mech. **52**, 571 (1985).
[19] Huajian Gao and James R. Rice, A first-order perturbation analysis of crack trapping by arrays of obstacles, J. Appl. Mech. **56**, 828 (1989).
[20] Anne Tanguy, Matthieu Gounelle, and Stéphane Roux, From individual to collective pinning: Effect of long-range elastic interactions, Phys. Rev. E **58**, 1577 (1998).
[21] D. Bonamy, S. Santucci, and L. Ponson, Crackling Dynamics in Material Failure as the Signature of a Self-Organized Dynamic Phase Transition, Phys. Rev. Lett. **101**, 045501 (2008).
[22] J. F. Joanny and P. G. de Gennes, A model for contact angle hysteresis, J. Chem. Phys. **81**, 552 (1984).
[23] Sébastien Moulinet, Alberto Rosso, Werner Krauth, and Etienne Rolley, Width distribution of contact lines on a disordered substrate, Phys. Rev. E **69**, 035103(R) (2004).
[24] P. Le Doussal, K. J. Wiese, S. Moulinet, and E. Rolley, Height fluctuations of a contact line: A direct measurement of the renormalized disorder correlator, Europhys. Lett. **87**, 56001 (2009).
[25] Jean-Christophe Baret, Damien Vandembroucq, and Stéphane Roux, Extremal Model for Amorphous Media Plasticity, Phys. Rev. Lett. **89**, 195506 (2002).
[26] Jie Lin, Edan Lerner, Alberto Rosso, and Matthieu Wyart, Scaling description of the yielding transition in soft amorphous solids at zero temperature, Proc. Natl. Acad. Sci. U.S.A. **111**, 14382 (2014).
[27] Oskar Hallatschek and Daniel S. Fisher, Acceleration of evolutionary spread by long-range dispersal, Proc. Natl. Acad. Sci. U.S.A. **111**, E4911 (2014).
[28] Shirshendu Chatterjee and Partha S. Dey, Multiple phase transitions in long-range first-passage percolation on square lattices, Commun. Pure Appl. Math. **69**, 203 (2016).

[29] Xiangyu Cao, Alberto Rosso, Jean-Philippe Bouchaud, and Pierre Le Doussal, Genuine localization transition in a long-range hopping model, Phys. Rev. E **95**, 062118 (2017).
[30] Haye Hinrichsen, Non-equilibrium critical phenomena and phase transitions into absorbing states, Adv. Phys. **49**, 815 (2000).
[31] Hans-Karl Janssen and Olaf Stenull, Field theory of directed percolation with long-range spreading, Phys. Rev. E **78**, 061117 (2008).
[32] Peter Grassberger, SIR epidemics with long-range infection in one dimension, J. Stat. Mech. (2013) P04004.
[33] Peter Grassberger, Two-dimensional sir epidemics with long range infection, J. Stat. Phys. **153**, 289 (2013).
[34] See Supplemental Material at http://link.aps.org/supplemental/10.1103/PhysRevLett.129.108301 for derivations, additional results, application to Covid infection data, and numerical methods, which includes Refs. [35–39].
[35] Pierre Le Doussal, More on the Brownian force model: Avalanche shapes, tip driven, higher d, arXiv:2203.10544.
[36] Leonid Mytnik and Edwin Perkins, The dimension of the boundary of super-brownian motion, Probab. Theory Relat. Fields **174**, 821 (2019).
[37] Onuttom Narayan and Daniel S. Fisher, Threshold critical dynamics of driven interfaces in random media, Phys. Rev. B **48**, 7030 (1993).
[38] S. Zapperi, P. Cizeau, G. Durin, and H. E. Stanley, Dynamics of a ferromagnetic domain wall: Avalanches, depinning transition, and the barkhausen effect, Phys. Rev. B **58**, 6353 (1998).
[39] Alexander Dobrinevski, Pierre Le Doussal, and Kay Jörg Wiese, Avalanche shape and exponents beyond mean-field theory, Europhys. Lett. **108**, 66002 (2014).
[40] For a recent review see Pierre Le Doussal, Equivalence of mean-field avalanches and branching diffusions: From the Brownian force model to the super-Brownian motion, arXiv:2203.10512.
[41] P. Le Doussal and K. J. Wiese, Distribution of velocities in an avalanche, Europhys. Lett. **97**, 46004 (2012).
[42] Pierre Le Doussal and Kay Jörg Wiese, Avalanche dynamics of elastic interfaces, Phys. Rev. E **88**, 022106 (2013).
[43] Knut Jørgen Måløy, Stéphane Santucci, Jean Schmittbuhl, and Renaud Toussaint, Local Waiting Time Fluctuations Along a Randomly Pinned Crack Front, Phys. Rev. Lett. **96**, 045501 (2006).
[44] Lasse Laurson, Stephane Santucci, and Stefano Zapperi, Avalanches and clusters in planar crack front propagation, Phys. Rev. E **81**, 046116 (2010).
[45] Clément Le Priol, Pierre Le Doussal, and Alberto Rosso, Spatial Clustering of Depinning Avalanches in Presence of Long-Range Interactions, Phys. Rev. Lett. **126**, 025702 (2021).
[46] D. Ertaş and M. Kardar, Critical dynamics of contact line depinning, Phys. Rev. E **49**, R2532 (1994).
[47] Pierre Le Doussal, Kay Jörg Wiese, and Pascal Chauve, Two-loop functional renormalization group theory of the depinning transition, Phys. Rev. B **66**, 174201 (2002).
[48] Alberto Rosso and Werner Krauth, Roughness at the depinning threshold for a long-range elastic string, Phys. Rev. E **65**, 025101(R) (2002).
[49] Thimothée Thiery, Pierre Le Doussal, and Kay Jörg Wiese, Spatial shape of avalanches in the brownian force model, J. Stat. Mech. (2015) P08019.
[50] A similar but less precise description applies to 2D if we replace a gap of length g by an "empty space" of area g^2.
[51] R. A. Fisher, The wave of advance of advantageous genes, Ann. Eugen. **7**, 355 (1937).
[52] A. Kolmogorov, I. Petrovsky, and N. Piscounov, Etude de l'équation de la diffusion avec croissance de la quantit é de matière et son application à un problème biologique, Bull. Univ. Etat Moscou A **1**, 1 (1937).
[53] D. A. Dawson, Stochastic evolution equations and related measure processes, J. Multivariate Anal. **5**, 1 (1975).
[54] Shinzo Watanabe, A limit theorem of branching processes and continuous state branching processes, J. Math. Kyoto Univ. **8**, 141 (1968).
[55] Xavier Cabré and Jean-Michel Roquejoffre, The influence of fractional diffusion in fisher-KPP equations, Commun. Math. Phys. **320**, 679 (2013).
[56] Clément Le Priol, Long-range interactions in the avalanches of elastic interfaces, Theses, Université Paris sciences et lettres, 2020.
[57] Dina Mistry, Maria Litvinova, Ana Pastore y Piontti, Matteo Chinazzi, Laura Fumanelli, Marcelo F. C. Gomes, Syed A. Haque, Quan-Hui Liu, Kunpeng Mu, Xinyue Xiong, M. Elizabeth Halloran, Ira M. Longini, Stefano Merler, Marco Ajelli, and Alessandro Vespignani, Inferring high-resolution human mixing patterns for disease modeling, Nat. Commun. **12**, 323 (2021).
[58] J. O. Lloyd-Smith, S. J. Schreiber, P. E. Kopp, and W. M. Getz, Superspreading and the effect of individual variation on disease emergence, Nature (London) **438**, 355 (2005).
[59] Martin Meyer, Shlomo Havlin, and Armin Bunde, Clustering of independently diffusing individuals by birth and death processes, Phys. Rev. E **54**, 5567 (1996).
[60] B. Houchmandzadeh, Neutral Clustering in a Simple Experimental Ecological Community, Phys. Rev. Lett. **101**, 078103 (2008).
[61] Joaquin Marro and Ronald Dickman, *Nonequilibrium Phase Transitions in Lattice Models*, Collection Alea-Saclay: Monographs and Texts in Statistical Physics (Cambridge University Press, Cambridge, England, 1999).
[62] Pavel L. Krapivsky, Sidney Redner, and Eli Ben-Naim, *A Kinetic View of Statistical Physics* (Cambridge University Press, Cambridge, England, 2010).
[63] https://anr.fr/Project-ANR-17-CE30-0027.